Geophysical Journal International

Geophys. J. Int. (2018) **214,** 2195–2206
Advance Access publication 2018 June 23
GJI Gravity, geodesy and tides

doi: 10.1093/gji/ggy254

Effects of unmodelled tidal displacements in GPS and GLONASS coordinate time-series

K. E. Abraha,[1] F. N. Teferle,[1] A. Hunegnaw[1] and R. Dach[2]

[1] *Geodesy and Geospatial Engineering, Institute of Civil Engineering and Environment, University of Luxembourg,* Luxembourg City, L-1359 *Luxembourg. E-mail: kibebuy@gmail.com*
[2] *Astronomical Institute, University of Bern, Sidlerstrasse* 5, CH-3012 *Bern, Switzerland*

Accepted 2018 June 21. Received 2017 September 14; in original form 2018 June 20

This study demonstrates the different effects of unmodelled (sub-)daily tidal displacement in Global Positioning System (GPS) and GLObalnaya NAvigatsionnaya Sputnikovaya Sistema (GLONASS) coordinate time-series. The results show that more than two propagated periodic signals appear in GPS and GLONASS Precise Point Positioning (PPP) coordinate time-series in the presence of an unmodelled M_2/O_1 tidal displacements as a result of a non-overlapping 24-hr data sampling. To summarize the propagated periodic signals at the fortnightly period, an unmodelled M_2 tidal displacement propagates predominately into two long-period signals at 13.6x (x is a positive integer) and 14.76 d for GPS, while only one significant propagated periodic signal at 14.76 d is discernible for GLONASS. Similarly, significant propagated periodic signals at 13.6x and 14.19 d for GPS and only at 14.19 d for GLONASS are evident as a result of an unmodelled O_1 tidal displacement. However, an unmodelled M_f (long-period) signal results in a strong power of similar magnitude at 13.6x d (∼13.66 d) for both GPS and GLONASS solutions. The appearance of different periodic signals as a result of the same unmodelled tidal displacement is attributed to the different ground repeat periods of the constellations. The latter is likely to explain the reason why the 13.6x-d fortnightly signal is present only in GPS solutions. Comparing the powers of the M_2 propagated periodic signals at 13.6x and 14.76 d on average from 32 globally distributed stations, the amplitude of the former is larger than for the latter by an order of magnitude. The results of this study demonstrate that the 13.6x-d periodic signal in GPS/GNSS (Global Navigation Satellite System) derived products is a joint contribution of the propagation of unmodelled (sub-)daily tidal displacements and errors at longer periods with the former appearing to contribute more. Significant reduction of the propagated periodic signals is achieved from combined-system solutions where including Galileo (the European GNSS) to the combined solution already shows benefits by reducing the effect even before the system has reached its full constellation. Combined GNSS solutions will benefit the applications of GNSS time-series for retrieving tidal harmonic signals such as M_f as they reduce constellation specific propagation effects.

Key words: Time-series analysis, Satellite geodesy, Space geodetic surveys.

1 INTRODUCTION

The potential use of Global Navigation Satellite System (GNSS) time-series for geophysical studies such as mean sea level monitoring and ground deformation has been demonstrated (Teferle *et al.*, 2006; Sella *et al.*, 2007; Teferle *et al.*, 2009; Bradley *et al.*, 2009; Santamaría-Gómez *et al.*, 2012). The reliability and accuracy of the time-series are essential for a complete understanding of the geophysical phenomena of interest. Understanding and mitigation of the technical (periodic) errors, which may cause erroneous interpretations of real geophysical signals, are therefore very important.

Pervasive annual and semi-annual variations (van Dam *et al.*, 2001; Dong *et al.*, 2002) and the harmonics of GNSS draconitics (Abraha *et al.*, 2017; Amiri-Simkooei *et al.*, 2007; Ray *et al.*, 2007) are the well-known long-period (LP) errors in GNSS coordinate time-series. Studies have also demonstrated short-period effects and subseasonal signals with fortnightly periods (Griffiths & Ray, 2012; Ray *et al.*, 2013; Abraha *et al.*, 2017).

The presence of several signals with fortnightly periods has been reported in nearly all GNSS products (Amiri-Simkooei *et al.*, 2007; Griffiths & Ray, 2012; Ray *et al.*, 2013; Abraha *et al.*, 2017). The largest fortnightly periodic signals which have been discussed previously are the 13.63/13.66- and 14.19/14.76-d ones.

Power centred at the fortnightly period appears in Global Positioning System (GPS) derived products because of three potential sources (Penna & Stewart, 2003; Stewart *et al.*, 2005; Penna *et al.*, 2007; Ray *et al.*, 2013). The first source can be mis-modelled LP tides, which were referred to as the 'direct effect' in some studies (Ray *et al.*, 2013). The two largest LP tides are the M_f tide and that with Doodson number 075565, with frequencies (and periods) of 0.07320 cycles d^{-1} (13.661 d) and 0.07335 cycles d^{-1} (13.633 d), respectively. For brevity we represent these and other periodic signals at this frequency as 13.6*x*-d.

The second potential source is the propagation of mis-modelled semi-diurnal and diurnal ((sub-)daily) tides because of the 24-hr sampling created by standard GPS data processing. We term those periodic signals as AP (aliased processing). The two largest powers are the AP(M_2) and AP(O_1) with frequencies (and periods) of 0.06777 cycles d^{-1} (14.755 d) and 0.07049 cycles d^{-1} (14.187 d), respectively.

Lastly, fortnightly periodic signals appear in GPS processing because of the propagation of mis-modelled (sub-)daily tides due to the ground repeat period of the GPS satellites. These periodic signals will be termed as PO (propagated orbit-repeat periodicities, which are orbit-repeat dependent propagations) throughout the paper. The two largest powers are the PO(M_2) and PO(O_1). The two latter sources have been demonstrated with simulated data by Penna & Stewart (2003). The substantial study by Stewart *et al.* (2005), however, showed the propagation mechanism as a two-stage process—Taylor series truncation errors of the functional model, which are then propagated as aliased periods due to the 24-hr data sampling. The complex propagation mechanism demonstrated by Stewart *et al.* (2005) indicated that more than two signals can be expected as a result of the two-stage process—not only the two periods per unmodelled constituent as in Penna & Stewart (2003). This was later confirmed by Penna *et al.* (2007), where more than two periodic signals were evident as a result of, for example, unmodelled M_2/O_1 tides in some stations. The propagation mechanism is not only dependent on the ground repeat period of a certain GNSS constellation but also on station location and the period of the unmodelled (tidal) displacement (Stewart *et al.*, 2005; Penna *et al.*, 2007; Tregoning & Watson, 2009). The above termed abbreviations, PO—to refer to the ground repeat period dependency and AP—for the 24-hr data sampling, will still be used to identify the main propagated signals according to the Stewart *et al.* (2005) mechanism.

One of the assumptions adopted in both Penna & Stewart (2003) and Stewart *et al.* (2005) is the constant GPS ground repeat period. The average ground repeat period of GPS is around 247 s less than a day (7.5 s longer than a sidereal day), which varies among satellites (Agnew & Larson, 2007) as it is affected by factors such as repositioning events and uncertainties in launch procedures. Consequently, broadened POs can be predicted. Estimating the GPS ground repeat period for each satellite using the routines of Agnew & Larson (2007) and predicting the resulting PO(M_2) and PO(O_1) using eq. (1) of Penna & Stewart (2003) shows periodic signals which vary among satellites. PO(M_2) and PO(O_1) for the different satellites range between 13.60 and 13.67 d.

Assuming the ground repeat periods of the satellites as random variables the POs will have a certain distribution. Using the ground repeat periods for all satellites every 5 d for the time span 2006–2018 inclusive—but shifting by 2 s to be closer to the aspect repeat times (Agnew & Larson, 2007)—the distribution of the PO(M_2) and PO(O_1) is estimated. Fig. 1 shows the distributions of the resulting aliases with median values of 26.8346 cycles yr^{-1} (13.6111 d) for PO(M_2) and 26.7859 cycles yr^{-1} (13.6359 d) for PO(O_1). Note that the simple propagation mechanism of Penna & Stewart (2003) is used to demonstrate the effect of different satellite orbit-repeat periods in Fig. 1. However, the effect of the variable satellite ground repeat period also applies for the two-stage propagation mechanism of Stewart *et al.* (2005).

As the ground repeat period of GLObalnaya NAvigatsionnaya Sputnikovaya Sistema (GLONASS) satellites is nearly eight sidereal days (Dach *et al.*, 2009), the POs presented in Stewart *et al.* (2005) and (Penna *et al.*, 2007) are not expected in the conventional 24-hr batch solutions. However, the APs, which are listed in table 1 of Penna & Stewart (2003) and table 1 of Griffiths & Ray (2012), will also apply for solutions computed using GLONASS observations and products. More than two propagated terms are predicted, for example for M_2/O_1, based on the GPS ground repeat period using eqs (30)–(33) of Stewart *et al.* (2005) and eq. (1) of Penna & Stewart (2003) as listed in table 1 of Penna *et al.* (2007). Using the same mechanism but with the ground repeat period of GLONASS, the theoretically predicted propagated periodic signals are presented in Table 1. Similar predictions are also included for the European GNSS (Galileo) for comparison. Note that those predictions are adopted by taking an average of the constantly repeating satellite geometries at nearly one, eight and ten sidereal days for GPS, GLONASS and Galileo, respectively. From Table 1 the propagated periods on the first row are those termed as APs and are the same for GPS, GLONASS and Galileo assuming the same 24-hr batch solutions. The other terms, on rows 2–5, are the propagated periods of the truncated errors as a result of the 24-hr sampling and these vary for each GNSS. The latter periodic signals are categorized under the POs as they are all ground repeat period dependent. No 13.6*x*-d periods are predicted for GLONASS and Galileo from unmodelled M_2/O_1.

Although the aforementioned main sources of the fortnightly periodic signal were predicted for GPS in theory (Stewart *et al.*, 2005) and have been demonstrated on simulated and real data (Penna & Stewart, 2003; Penna *et al.*, 2007), the effects on GLONASS have not been investigated previously. This study contributes in demonstrating the latter. Moreover, it demonstrates that comparing GPS and GLONASS solutions can be used as a means to identifying the main source of the strong fortnightly periodic signals observed in GPS/GNSS-derived products.

The 13.6*x*-d periodic signal is an important feature as it may indicate the underlying deficiencies of the standard tidal models used as a priori in GNSS data processing. Moreover, understanding the short-period signals in GNSS coordinate time-series is essential for a complete understanding of geophysical processes and for the developments of GNSS-based strategies for natural hazard warnings, for example, tsunami and earthquake warnings (Blewitt *et al.*, 2009; Melgar *et al.*, 2016).

Section 2 describes the details of the GNSS data processing strategy used in this study. The results are presented in Section 3, which is divided into three different subsections. This study was motivated by Abraha *et al.* (2017), who have reported that the 13.6*x*-d periodic signal, which is assumed to be mainly caused by LP (Ray *et al.*, 2013; Rebischung *et al.*, 2016), is not discernible in GLONASS Precise Point Positioning (PPP) coordinate time-series while it clearly exists for GPS. Hence, to confirm and demonstrate this, Section 3.1 briefly compares PPP solutions from GPS and GLONASS observations. Section 3.2 investigates the orbit overlaps of GPS and GLONASS satellites separately to support the results in Section 3.1. In Section 3.2, the effects of unmodelled (sub-)daily tidal displacement on GLONASS coordinate time-series are investigated and compared to those for GPS. Although the main results

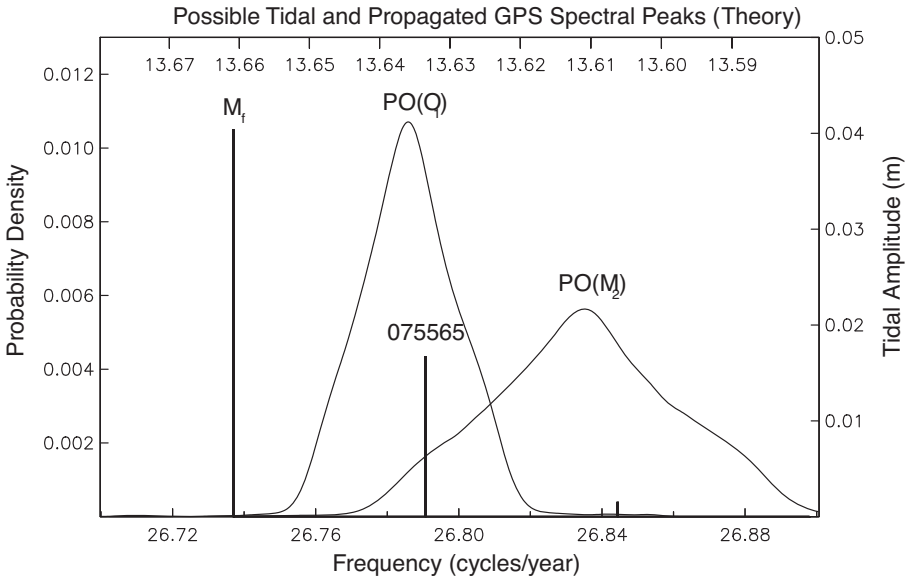

Figure 1 Propagated and long-period signals for GPS near the fortnightly tide. The propagated signals are shown as a probability density (left scale) that gives the distribution of them, computed from the orbit repeat times for all satellites from 2006.0 through 2018.0, with 2 s added to match the aspect repeat time of Agnew & Larson (2007). The median values for these distributions are 26.8346 cycles yr^{-1} (13.6111 d) for the M_2 tide, and 26.7859 cycles yr^{-1} (13.6359 d) for the O_1 tide. The long-period tides (M_f and that with Doodson number 075565) are shown as spikes in frequency, with the amplitudes (right-hand scale) they would produce in vertical displacement, using the normalization of Cartwright & Tayler (1971).

Table 1. Predicted periods (in days) from propagations of unmodelled M_2/O_1 using eqs (30)–(33) of Stewart *et al.* (2005) and eq. (1) of Penna & Stewart (2003) for GPS, GLONASS and Galileo. Only the 1st to 5th terms are presented in this table. Note that an average of constantly repeating satellite geometry at sidereal day (23.934471 hr) for GPS, eight sidereal days (191.475775 hr) for GLONASS and ten sidereal days (239.344719 hr) for Galileo are adopted and used in eqs (30)–(33) of Stewart *et al.* (2005).

	M_2			O_1		
	GPS	GLONASS	Galileo	GPS	GLONASS	Galileo
1st	14.765	14.765	14.765	14.192	14.192	14.192
2nd	13.661	3.141	3.728	13.168	3.114	3.690
3rd	16.064	5.466	7.529	15.387	5.549	7.687
4th	14.192	5.180	5.952	13.661	5.107	5.857
5th	15.387	17.356	30.724	14.765	18.222	33.546

and conclusions of this study are based on GPS and GLONASS solutions, GPS+GLONASS and GPS+GLONASS+Galileo combined solutions are also briefly presented in this section for comparison. Section 4 summarizes the main points and concludes the study.

2 GNSS DATA PROCESSING

PPP (Zumberge *et al.*, 1997) solutions were generated using GPS and GLONASS observations and products in the Bernese GNSS Software version 5.2 (BSW52; Dach *et al.*, 2015) in a non-overlapping 24-hr data sampling. GNSS satellite orbits, clocks and Earth Rotation Parameters (ERPs) were taken from two International GNSS Service (IGS; Dow *et al.*, 2009) analysis centres (ACs), namely the Center for Orbit Determination in Europe (CODE) and the European Space Agency (ESA). These two ACs generate combined GPS+GLONASS solutions from which the GPS and GLONASS satellite products are extracted for our single-system PPP solutions. The satellite orbits, clocks and ERPs were then held fixed in the PPP solutions, with station coordinates, troposphere parameters and receiver clock offsets estimated.

Undifferenced phase and code observations were used in the processing with the latter having a lower weight. Observations above 3° elevation cut-off were employed with elevation-dependent weighting scheme ($\frac{1}{\cos^2 z}$, z is zenith angle) applied. Satellite and receiver antenna phase centre corrections were applied based on GNSS-specific calibrations where, if no corrections were included for GLONASS the corresponding values from GPS were used. The FES2004[1] ocean tide loading (OTL) was used to correct tidal displacement, and Earth and polar tides were corrected according to the International Earth Rotation and Reference Service (IERS) convention 2010 (Petit & Luzum, 2010). However, only ambiguity float solutions were generated for both GPS and GLONASS. More details of the PPP strategy used in this study can be found in table 1 of Abraha *et al.* (2017).

3 RESULTS

3.1 PPP coordinate time-series

Two separate single-system PPP solutions were produced using GPS and GLONASS observations on a global set of 32 stations (Fig. 2) for 2012.0–2016.0. Each solution was computed twice using CODE[2] and ESA[3] products. For the solutions in this specific section ESA products from the IGS 2nd data reprocessing campaign (repro2)[4] were used while for CODE the product series from a new reprocessing (Susnik *et al.*, 2016) were employed as the operational

[1] http://holt.oso.chalmers.se/loading/
[2] ftp://ftp.aiub.unibe.ch/REPRO_2015/CODE_REPRO_2015.ACN
[3] ftp://ftp.igs.org/pub/center/analysis/esa.acn
[4] repro2 is an IGS reprocessing campaign which re-analysed full history of GNSS data since 1994. More information can be found at: http://acc.igs.org/reprocess2.html

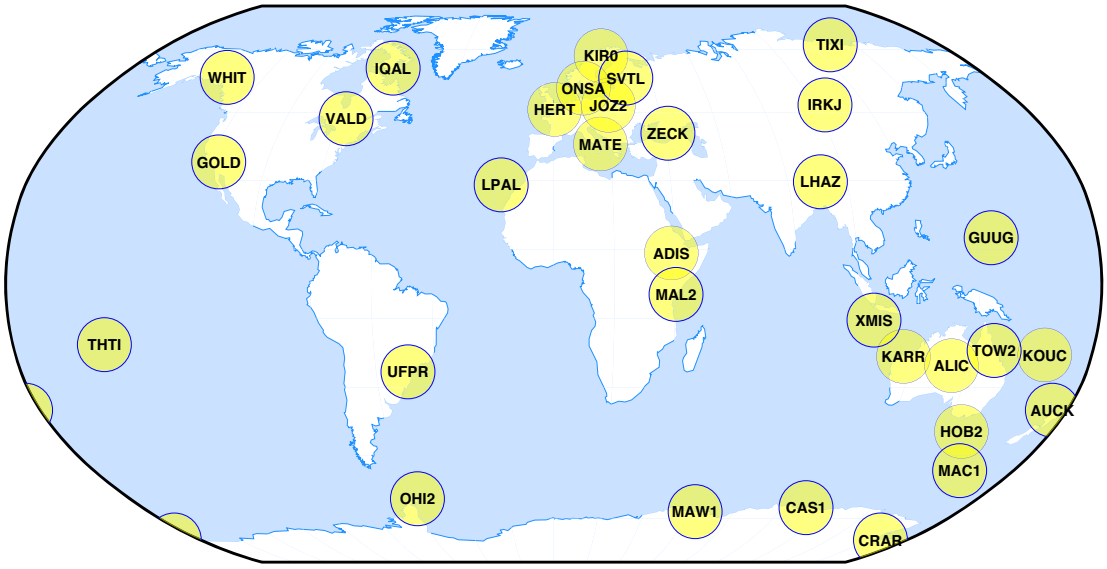

Figure 2 Map of selected IGS stations with GPS and GLONASS observations.

and repro2 products did not include GLONASS satellite clocks for the period of interest. The coordinate time-series of the stations were then analysed (detrended, outliers removed and offsets, if any present, corrected). These cleaned time-series were then used as an input to compute the associated power spectra. The spectra of all stations were stacked and plotted as power versus frequency (Fig. 3). Fig. 3 shows the stacked spectra for both GPS (upper panels) and GLONASS (lower panels) solutions using products from both CODE and ESA. The vertical dashed lines in the figure show the 13.6*x*-, 14.19-, 14.76- and 8-d periodic signals in the upper panels and the additional 4- and 2.67-d periodic signals in the lower panels.

A stochastic analysis of the time-series showed that a combination of flicker and white noise characterizes the general picture of the background spectra for both GPS and GLONASS solutions (results not shown here). Plotted in Fig. 3 are the higher frequency sections of the spectra as the objective of this study is to inspect the high frequency periodic features. The lower frequency regions of the spectra can be seen in Abraha *et al.* (2017). From Fig. 3, the main periodic features of the GPS solutions are at 13.6*x* and 8 d. Weak AP(M_2) power is an additional feature which can be seen in a closer inspection, while the AP(O_1) power is faint. The 13.6*x*-d periodic signal is clearly visible from the GPS solutions. Some studies such as Ray *et al.* (2013) postulated that this periodic signal was linked to LP errors. The 8-d period is a GLONASS-specific feature, which is linked to the ground repeat period (8 sidereal days) of the constellation. The existence of the 8-d periodic signal in the GPS solutions is an indication that GPS orbits produced from a combined GPS+GLONASS solution contain GLONASS-specific periodic signals as Abraha *et al.* (2017) were able to show.

The main features of the GLONASS solutions are the clear 14.76-, 8-d periodic signals and the associated second and third harmonics, and the absence of the 13.6*x*-d periodic signal. Those features were also reported by Abraha *et al.* (2017) using ESA products. Similar features are confirmed here when employing CODE products. The clear peaks of the 8-d periodic signal and its second (∼4-d) and third (∼2.67-d) harmonics indicate the reappearance of errors due to the ground repeat period of the GLONASS constellation. Abraha *et al.* (2017) have also demonstrated that the evolving GLONASS constellation is found to be contributing to the powers at some of the frequencies. As the GLONASS constellation was complete since December 2011, the PPP solutions in this study are from 2012 January 1 onwards to reduce those effects.

The features which are common for both GPS and GLONASS solutions are the AP(M_2/O_1). The AP(O_1) is faint in both solutions. The reason can be related to the weak power of the signal. The AP(M_2) is visible (mainly in the horizontal components) in both solution types but is more clearly seen for the GLONASS solution. The faint nature of the AP(M_2/O_1) in the vertical component was also found for the latest repro2 solution from nearly all ACs (Rebischung *et al.*, 2016).

A feature which is not common for both GPS and GLONASS solutions is the 13.6*x*-d in addition to the 8-d periodic signal and its harmonics. The 8-d periodic signal is a clear indication of a GLONASS-specific systematic effect, as has been stated above and was demonstrated by previous studies (Ray *et al.*, 2013; Abraha *et al.*, 2017). However, the absence of the 13.6*x*-d signal in the GLONASS solution is unexpected if one assumes that LPs are the main cause. For similar inspections of the effect we have looked at the spectra of the orbit overlaps for both GPS and GLONASS orbits. Previous studies reported that a comb at the fortnightly periodic signal is evident in the GPS orbit overlaps (Griffiths & Ray, 2012; Ray *et al.*, 2013; Rodriguez-Solano *et al.*, 2014).

3.2 Spectra of orbit overlaps

Orbit overlaps were computed for GPS and GLONASS satellites using CODE & ESA repro2 and IGS operational products. As the true values of the orbits are not known, orbit overlaps are one way of assessing the internal orbit consistency and precision (e.g. Griffiths & Ray, 2012; Rodriguez-Solano *et al.*, 2014; Arnold *et al.*, 2015). The orbit overlaps of the satellite's Cartesian positions were estimated at the day boundaries for 2008.0–2016.0. As the satellite orbit arcs are given every 15 min from 00:00:00 to 23:45:00, the first arc was extrapolated to midnight (00:00:00) and compared with the satellite's orbit arc for the next day. The spectra of the orbit overlap time-series were computed for each individual satellite, and then

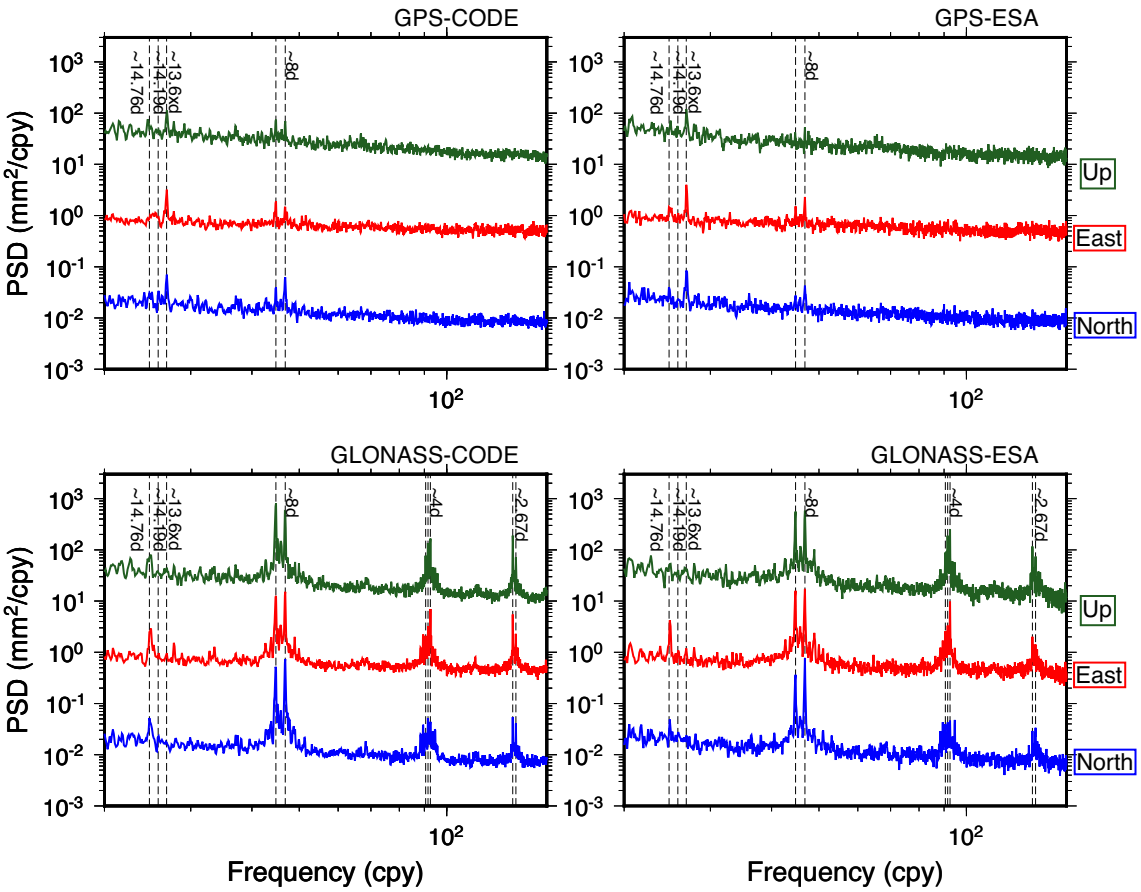

Figure 3 Stacked and normalized power spectra of GPS (upper panel) and GLONASS (lower panel) PPP solutions from both CODE (left panel) and ESA (right panel) products for stations in Fig. 2. The vertical dashed lines show fortnightly (14.76-, 14.19- and 13.6*x*-d periodic signals) and the GLONASS-specific 8-d periodic signal and its second and third harmonics (4- and 2.67-d periodic signals). The spectra are computed for north, east and up components (see colour codes) and the high-frequency section is plotted with a shift along the vertical axis for clarity.

stacked for all satellites. This was done for GPS and GLONASS satellites separately using CODE, ESA & IGS and CODE & ESA products, respectively. The satellite orbits used for the estimations of the orbit overlaps were from a 1-d arc. Eclipsed satellites were also included in the stacked spectra as excluding them showed no significant differences.

Fig. 4 shows the high-frequency section of the normalized power of the stacked spectra versus period (days). The dotted vertical lines show a 7-d periodic signal and its second (3.5-d period) and third (2.33-d period) harmonics, the dashed vertical lines show an 8-d periodic signal and its second and third harmonics, and the black box shows the broad distribution of lines around the fortnightly (∼14-d) periodic signal. The background noise of the full spectra is characterized by a combination of power law and white noise with the latter dominating the high-frequency region depicted in the figure. Moreover, harmonics of draconitic periodic signals are evident for both GPS and GLONASS (results not shown here). The main short-period features in Fig. 4 are the pronounced broad fortnightly periodic signal (as also in Griffiths & Ray, 2012; Rodriguez-Solano *et al.*, 2014), the 7-d periodic signal and its harmonics from the GPS orbit overlaps, and the broad 8-d periodic signal and its second and third harmonics from the GLONASS orbit overlaps. From the GLONASS orbit overlaps the absence of the fortnightly periodic signal is evident.

The 7-d periodic signal and its second and third harmonics are present only in the GPS orbit overlaps. As these periods are not discernible for GLONASS, their presence in the GPS orbit overlaps can be related to unabsorbed effects of the orbit model fitting while computing the overlaps. For now, this is the only postulation we can make and we do not provide any further hypothesis rather than reporting its presence. A pronounced and (very) broad 8-d comb and its second and third harmonics are evident from the GLONASS orbit overlaps—systematic errors reappear due to the satellites ground repeat period. Those periodic signals were also seen by Rodriguez-Solano *et al.* (2014) and using better solar radiation pressure modelling appears to be reducing the powers to some extent. As the main goal of the orbit overlap analysis in this study is to inspect the fortnightly periodic signal, no more discussions on the 8- and 7-d periodic signals will be added here.

Although a broad peak for the fortnightly periodic signals exists in the GPS orbit overlaps, it is not discernible in the corresponding case for GLONASS. The results presented in this section and Section 3.2 suggest that POs, compared to LPs, can indeed be the main contributors of the fortnightly periodic signals in GPS-derived products. To strengthen this hypothesis and for further investigations on the 13.6*x*-d periodic signal, the effect of unmodelled (sub-)daily tidal displacements is examined on GLONASS PPP coordinates compared to those for GPS.

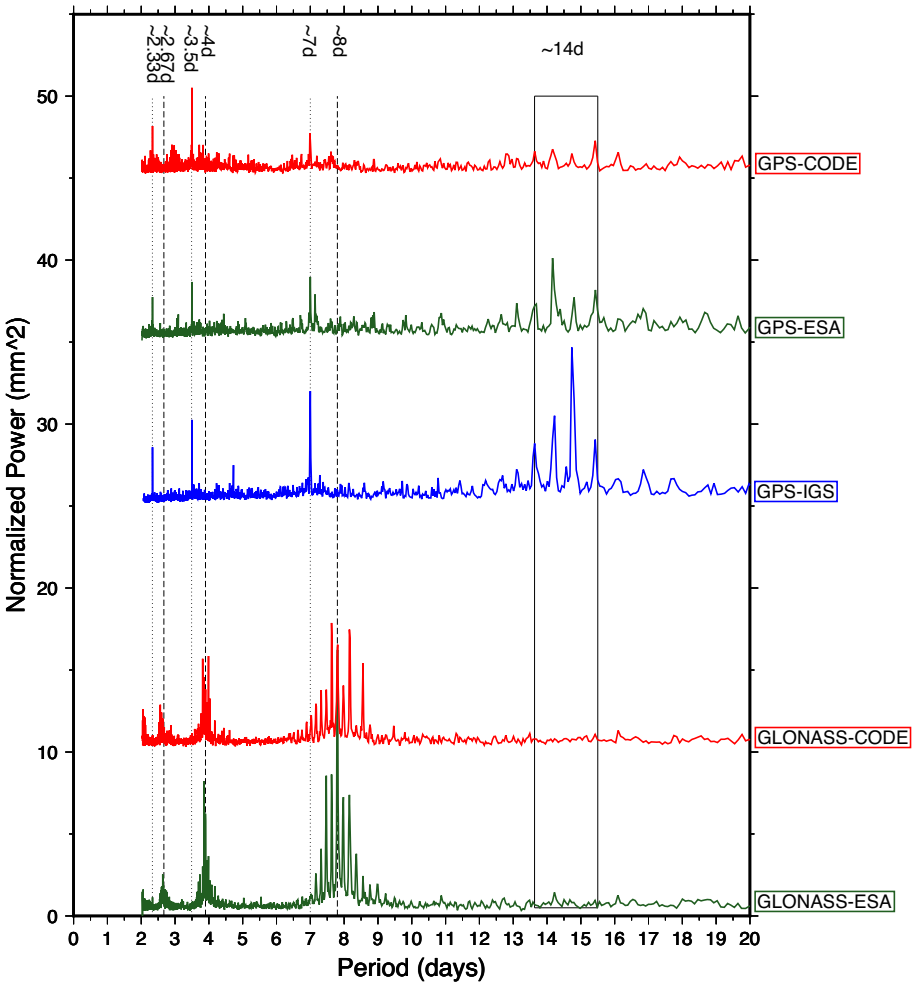

Figure 4 A plot of power spectra of (3-D) orbit overlaps versus period (days) for GPS and GLONASS satellites. The spectra of the orbit overlaps are computed for CODE (both GPS and GLONASS), ESA (both GPS and GLONASS) repro2 and IGS (GPS) operational products and plotted with a shift along the vertical axis for clarity. Vertical dotted lines show a 7-d periodic signal and its second and third harmonics (at 3.5 and 2.333 d), vertical dashed lines show an 8-d periodic signal and its second and third harmonics (at 4 and 2.67 d) and the black box shows a fortnightly periodic signal (∼14 d).

3.3 Effects of unmodelled (sub-)daily errors in GPS and GLONASS coordinate time-series

To investigate the effect of unmodelled (sub-)daily tidal displacements in GLONASS coordinate time-series in comparison to GPS, four non-overlapping daily (24-hr data sampling) PPP solutions were generated for 2012.0–2016.0 for both GPS and GLONASS. The first (reference) solution is based on PPP, as in Section 3.1, with all 11 constituents of OTL modelled, namely M_2, S_2, N_2, K_2, K_1, O_1, P_1, Q_1, M_f, M_m and S_{sa}, and the expanded set of tidal constituents as derived by the hardisp.f program (Petit & Luzum, 2010, p. 110). The second, third and fourth solutions were generated without M_2, O_1 and M_f corrections, respectively. When one constituent is not corrected, the effect of that constituent on the tidal displacement is also ignored and hence the final computed tidal displacement is only from the rest of the constituents. The coordinates generated from the three scenarios were then subtracted from the reference solution. As all other models and $(\text{CODE})^2$ products are the same for all solutions, the coordinate differences between the reference and the other solutions reveal the effects of the corresponding unmodelled tidal waves. This method was used by Penna *et al.* (2007) and is suitable for testing the effect of unmodelled (sub-)daily periods.

Although the effects were evident in all coordinate components, only the up component is presented here for brevity and as the effect is larger (Penna *et al.*, 2007). Fig. 5 shows the effect of the unmodelled M_2 tidal constituent on the up coordinate component for GPS (blue line) and GLONASS (red line) solutions. The coordinate differences (unmodelled M_2 effect) and their corresponding power spectra were computed for each individual station. The power spectra of all stations were then stacked and plotted in Fig. 5 as power versus period (days). The dashed vertical lines indicate the periods at 13.6x and 14.76 d.

Two main features centred at the fortnightly period, which are the 13.6x-d and 14.76-d periodic signals, are evident in Fig. 5. The 14.76-d periodic signal is the AP(M_2). The periodic signal is present in both GPS and GLONASS solutions as also predicted in Table 1. An interesting feature in Fig. 5 is the strong 13.6x-d periodic signal for GPS which is faint for GLONASS. This is PO(M_2) as also predicted in Table 1. Theoretically, the periodic signal is not expected to exist in the GLONASS solution as the ground repeat period is eight sidereal days, which is also confirmed here with real data. A close inspection of the unmodelled effects for individual stations shows an effect for all stations with the powers varying among stations. The power variation among stations is attributed

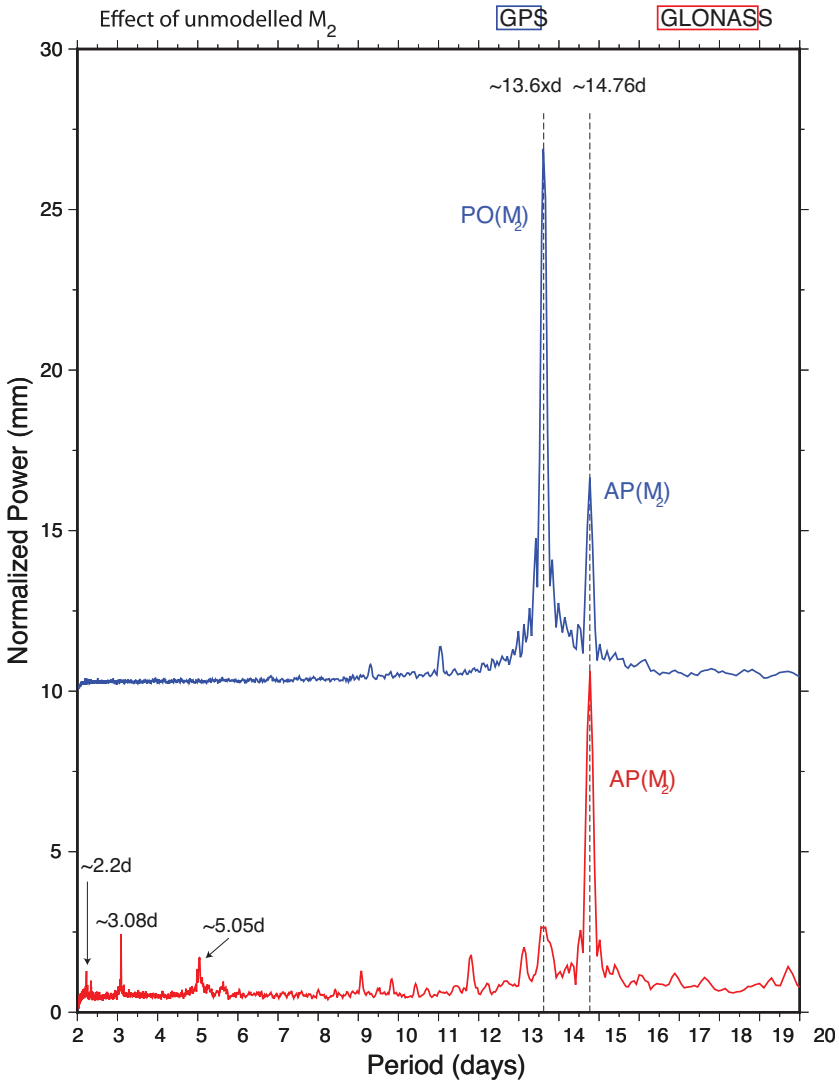

Figure 5 Effects of unmodelled M_2 OTL constituent on the (up) coordinate component for GPS (blue line) and GLONASS (red line) solutions. The normalized powers versus periods (days) are plotted with a shift along the vertical axis for clarity. The vertical dashed lines show the 13.6*x*-d and 14.76-d periodic signals.

to the dependency of the propagated errors on the magnitude of the unmodelled displacement, site locations, and the relative size between the horizontal and vertical displacements (Stewart *et al.*, 2005; Penna *et al.*, 2007). There are more interesting features (POs) of low power in Fig. 5 which are particular to GLONASS, namely periodic signals at ∼2.2, ∼3.1 and ∼5.1 d. The two latter periodic signals are predicted from the two-stage propagation mechanism of Stewart *et al.* (2005) as in Table 1. This is an interesting confirmation of the propagation mechanism with real data on two different GNSS. There are some artefacts but with very weak power at periods near to ∼9.3 and ∼11.2 d for GPS, ∼9.1 and ∼11.8 d for GLONASS which cannot be explained by the propagation mechanism from Stewart *et al.* (2005). On a closer inspection, these artefacts are not visible for some stations while they exist for others.

Fig. 6 shows a plot of power versus period of the effect of the unmodelled O_1 tidal constituent on the up component for both GPS (blue line) and GLONASS (red line) solutions. The dashed vertical lines indicate the 13.6*x*- and 14.19-d periodic signals. At the fortnightly period there are two main features which are the 13.6*x*- and 14.19-d periodic signals. The 14.19-d periodic signal is the AP(O_1) and is clearly visible in both GPS and GLONASS solutions as also predicted in Table 1. The 13-6*x*-d periodic signal strongly exists in the GPS solution (which is PO(O_1)) but is absent for GLONASS. This is again due to the ground repeat period differences of the systems, where PO(O_1) at 13.6*x* d is evident for GPS but not for GLONASS. As in Fig. 5 and predicted in Table 1 there are more features of low power, which are only present in the GLONASS solution. These include periods at ∼3.1 and ∼5.1 d. The ∼3.1-d signal is very weak compared to the ∼5.1-d one but can be seen clearly on a closer inspection. These two periods are predicted in Table 1 using the two-stage propagation mechanism of Stewart *et al.* (2005).

The above results, also in agreement with Penna *et al.* (2007), indicate that in GPS coordinate time-series it is difficult to identify if the 13.6*x*-d periodic signal is caused by PO(M_2) or PO(O_1). As a matter of fact, the LP(M_f/075565) tidal effects have powers at 13.6*x*-d in the coordinates as well, which makes it difficult to detect whether the 13.6*x*-d periodic signal is PO(M_2/O_1) or LP(M_f/075565) effect. To see the effect of an unmodelled LP(M_f), a third PPP solution was generated for GPS and GLONASS by modelling all other short- and LP effects but M_f. Fig. 7 shows a plot of power versus period (days) of the spectra of the (up) coordinate differences between

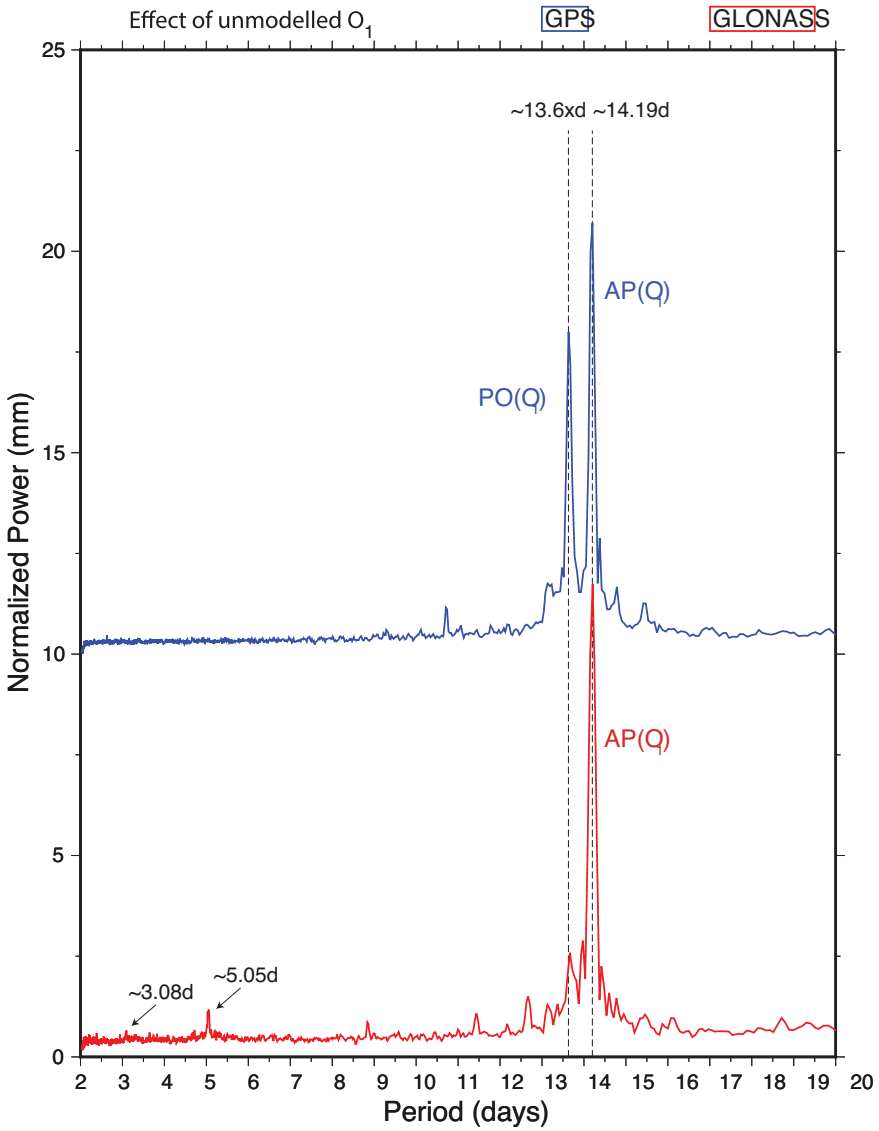

Figure 6 Effect of unmodelled O_1 OTL constituent on the (up) coordinate component for GPS (blue line) and GLONASS (red line) solutions. The normalized powers versus periods (days) are plotted with a shift along the vertical axis for clarity. The vertical dashed lines show the 13.6*x*- and 14.19-d periodic signals.

the reference solution and the PPP solution without M_f correction for both GPS (blue line) and GLONASS (red line) solutions. Interestingly, three features are evident in both GPS and GLONASS solutions showing similar power for both systems. The main signal is the 13.6*x*-d (13.66-d) period which is expected if the M_f constituent is unmodelled. Two weak powers at 9.13 and 14.78 d are also evident from the unmodelled M_f effect.

The 14.78-d periodic signal in Fig. 7 can be partially explained using the Stewart *et al.* (2005) mechanism. For GPS, an unmodelled effect at 13.66-d appears in the coordinate time-series at 13.66-d as a main periodic signal with more POs nearly at 14.76, 12.71, 14.19 and 13.16 d as a result of 24-hr batch processing. The ∼14.76-d periodic signal is only evident here. The Stewart *et al.* (2005) mechanism, however, does not explain the presence of the same periodic signal in GLONASS and the 9.13-d periodic signal in both GNSS. No more explanations of these features are given here at this stage. On a summary of the above experiments, however, it is worth mentioning that most of the periodic signals could be well explained by the Stewart *et al.* (2005) two-stage propagation mechanism.

Comparing the results of Figs 5, 6 and 7 shows that propagated unmodelled M_2/O_1 tidal displacements and unmodelled LP(M_f) have powers at the 13.6*x*-d period in the coordinate times series derived from GPS. However, only the unmodelled LP(M_f) shows a significant impact for the GLONASS observations of this period. The effects demonstrated for GLONASS also apply for other GNSS with long ground repeat periods such as Galileo and the Chinese BeiDou System, which have ground orbit repeat periods of 10 and 7 sidereal days, respectively.

The 3-D (averaged over all components) admittances (ratios of amplitudes of output to input) of the unmodelled M_2 tide for the 13.6*x*-d periodic signal (in the GPS solution) are 5–30 per cent for 78 per cent of the stations used in this study. Few stations show higher admittances of 35–60 per cent with one station (THTI, Tahiti, French Polynesia) showing 124 per cent admittance. However, the 14.76-d periodic signal has 5–12 per cent admittance for 97 per cent of the stations for both GPS and GLONASS solutions. This shows, for the GPS coordinate time-series that the power of PO(M_2) is larger than AP(M_2), which confirms Penna *et al.* (2007) but with

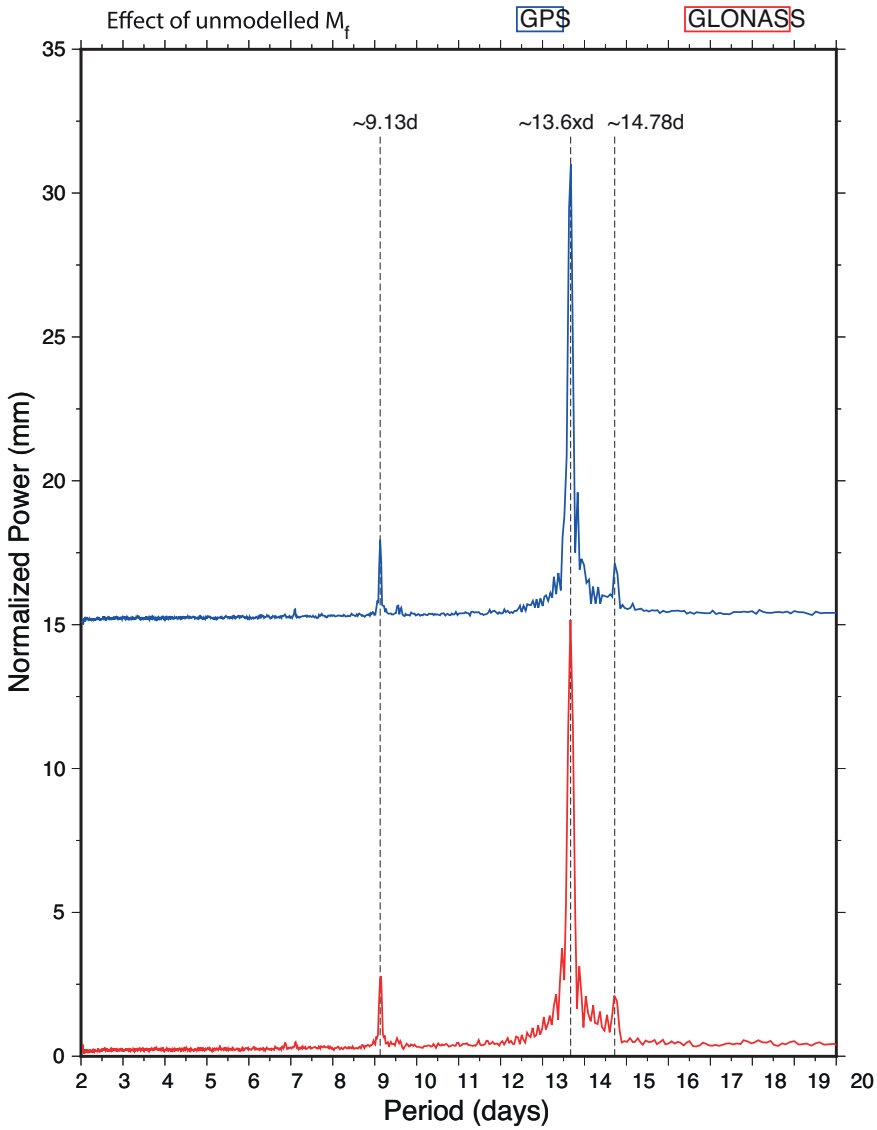

Figure 7 Effect of unmodelled M_f OTL constituent on the (up) coordinate component for GPS (blue line) and GLONASS (red line) solutions. The normalized powers versus periods (days) are plotted with a shift along the vertical axis for clarity. The vertical dashed lines show the 9.13-, 13.6*x*- and 14.78-d periodic signals.

more observations. Comparing the powers of the 13.6*x*- and 14.76-d periodic signals of the stacked spectra in Fig. 5, the amplitude of PO(M_2) is larger than for AP(M_2) by an order of magnitude. Inspecting station by station, however, three stations (CRAR, OHI2 and TIXI) show slightly larger amplitudes for the 14.76-d than for the 13.6*x*-d periodic signal. These admittance differences among stations indicate the station location dependency of the Stewart *et al.* (2005) propagation mechanism. However, from the stacked spectra in Fig. 6, the amplitude of AP(O_1) is 32 per cent larger than that of PO(O_1).

The results of this section demonstrate that a comparison of GPS and GLONASS solutions can be used as a means to identifying whether the POs and/or LPs are the main sources of the fortnightly (13.6*x*-d) periodic signal. Moreover, combined GNSS solutions reduce the magnitudes of propagated signals. Fig. 8 shows the effect of unmodelled M_2 on daily single-system GPS, and combined-systems GPS+GLONASS and GPS+GLONASS+Galileo PPP solutions. The power spectra of the (up) coordinate differences were stacked and plotted in this figure as blue (GPS), red (GPS+GLONASS) and green (GPS+GLONASS+Galileo) lines. The coordinate differences were equally normalized and plotted as power versus period. The power of PO(M_2) is well reduced in the combined solutions. Including Galileo to the combined solution already shows benefits by reducing the effect of error propagation even before the system has reached its full constellation. For this specific experiment, including GLONASS observations reduces the magnitude of PO(M_2) by 45 per cent while including both GLONASS and Galileo observations reduces the power by ∼52 per cent. New features which are not present in Fig. 5 appear at periods near to ∼2.11, ∼4.4 and ∼5.76 d by including Galileo to the combined solution (see inset in Fig. 8). A period near to the latter (∼5.96 d) is predicted in Table 1. A ninth-term periodic signal near to ∼4.2 d with nearly zero power can be predicted for Galileo using eqs (30)–(33) of Stewart *et al.* (2005). This may not explain the periodic signal at ∼4.4 d which is clearly visible in Fig. 8. Moreover, as the results presented in Fig. 8 were generated from the combination of all three systems, with

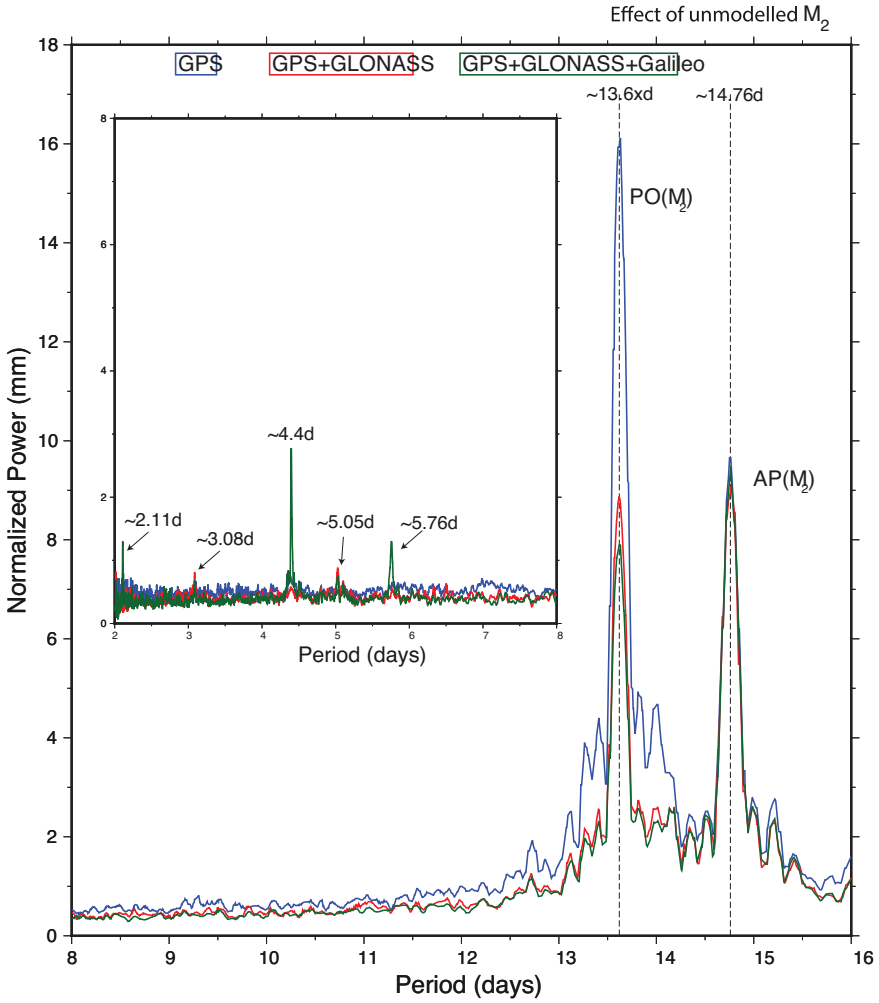

Figure 8 Effect of unmodelled M_2 OTL constituent on the (up) coordinate component for GPS, combined GPS+GLONASS and combined GPS+GLONASS+Galileo solutions. Vertical dashed lines are as in Fig. 5. The inset shows 2–8 d (period).

GPS and GLONASS dominating Galileo in terms of the number of observations, a Galileo-only solution may explain the effect better once the system reaches its full constellation.

Note that for the result in Fig. 8 a new set of 32 global stations different from Fig. 2 were selected as not all former stations were capable of observing Galileo. However, it should be noted that the same data set and processing settings were again employed for the GPS, GPS+GLONASS and GPS+GLONASS+Galileo results in this figure. Moreover, the PPP solutions were generated for 2014.0 to 2017.5 to make use of more Galileo observations. For this period the number of Galileo satellites[5] ranged between 4 in January 2014.0 and 17 in July 2017.

4 DISCUSSION AND CONCLUSION

This paper demonstrates that unmodelled (sub-)daily periods propagate to more than two longer periods in GPS and GLONASS coordinate time-series. For GPS the shortest propagated periods are nearly at the fortnightly period while for GLONASS propagated periods as short as 2–14 d appear from unmodelled M_2/O_1. The findings are in agreement with previous studies (Stewart *et al.*, 2005; Penna *et al.*, 2007) and the propagation mechanism from Stewart *et al.* (2005) explains most of the propagated signals. The presence of some of the predicted periods using eqs (30)–(33) of Stewart *et al.* (2005) on GLONASS (and Galileo) coordinate time-series is a confirmation of the propagation mechanism from a non-GPS constellation. Although the Stewart *et al.* (2005) mechanism was derived for two dimensions only and adopted some simplified assumptions, the GPS (also in agreement with Penna *et al.* (2007)) and GLONASS results presented here indicate that the mechanism still explains most of the propagated features in both GPS and GLONASS coordinate time-series.

A prominent fortnightly (mainly 13.6*x*-d) periodic signal resides in GNSS-derived products. Comparing GPS and GLONASS coordinate time-series, with the presence of the 14.19- and 14.76-d periodic signals in both solutions but the 13.6*x*-d periodic signal in the GPS solution only, the results may hint as to whether the (main) sources of the 13.6*x*-d periodic signal in GNSS products are LPs or propagated (sub-)daily errors. Unmodelled M_2/O_1 tidal displacements propagate into periods with 14.76/14.19 and 13.6*x* d for GPS but only into periods with 14.76/14.19 d for GLONASS in addition to the other features presented in Figs 5 and 6. The 13.6*x*-d periodic signal is faint in the GLONASS solution when there are M_2/O_1

[5]Galileo constellation status: http://mgex.igs.org/IGS_MGEX_Status_GAL.php

unmodelled effects. However, when there is an unmodelled LP effect, for example, M_f tidal constituent, a strong 13.6*x*-d periodic signal is evident in both GPS and GLONASS solutions.

Accordingly, we hypothesize that the main source of the 13.6*x*-d periodic signal reported in GNSS based products can be the propagated unmodelled (sub-)daily tides with both propagated (sub-)daily and unmodelled LP tides contributing to the power. The propagation mechanism described in Stewart *et al.* (2005) explains most of the propagated periodic signals from unmodelled subdaily tidal displacements in GNSS coordinate time-series. This was confirmed as more than two periodic signals appear as a result of a single unmodelled tidal displacement. The propagation mechanism of Stewart *et al.* (2005) was found to be dependent on station location, the period of the unmodelled periodic displacement but mainly on the ground repeat periods of satellites. The latter dependency was well explained with the real data in this study while the other dependencies are also confirmed here in agreement with other studies (Penna *et al.*, 2007; Tregoning & Watson, 2009).

These findings are essential on understanding the main source of the 13.6*x*-d periodic signal in GNSS derived products. However, a conclusive claim on the source of the periodic signal requires more experiments and assessments on the propagation mechanisms of other tidal models such as the EOPs. The periodic signal has different powers (propagation levels) among IGS ACs as the transfer mechanism of the propagated periodic signals is highly affected by their orbit modelling details and parametrization such as ambiguity resolution (Tregoning & Watson, 2009). Moreover, we cannot be fully conclusive on the nature and the main sources of the fortnightly features of the IGS solutions as they are produced using different software packages with some modelling differences.

The use of GPS time-series for retrieving tidal harmonic signals (King, 2006; Yuan *et al.*, 2009; Penna *et al.*, 2015; Martens *et al.*, 2016) and the implications for mantle anelasticity (Bos *et al.*, 2015; Kang *et al.*, 2015) have been well demonstrated. Most of the GPS-based studies demonstrated the estimations of the major (sub-)daily ocean tidal signals using either kinematic or static GPS data processing approaches. The use of daily GPS time-series for the estimation of LP tidal waves such as M_f can be contaminated by the propagation of the (sub-)daily periods such as M_2 and O_1.

Kang *et al.* (2015) carried out much work on the estimation of fortnightly and monthly body tides using GPS daily solutions from a global set of stations. They have demonstrated the possible contamination of their estimated M_f body tide from OTL errors and the propagation of (sub-)daily OTL waves. For the latter, however, they have only assumed periodic signals at 14.76 and 14.19 d, which are the AP(M_2) and AP(O_1), respectively. They have demonstrated that their long time-series allowed them to resolve the above mentioned periodic signals from the exact M_f period. However, they have not considered the PO(M_2/O_1), which may coincide with the M_f periodic signal. The effects of the POs in addition to the APs should be considered when the estimations of body and/or ocean tide M_f are to be made using daily GPS time-series. Combined GNSS solutions benefit the applications of GNSS time-series for such geophysical applications as they reduce the constellation specific effects (Fig. 8). It is also worth mentioning that reductions in the uncertainties of the 13.6*x*-d signals may also be achieved with different Green's function than the standard Green's function based on Gutenberg-Bullen Earth model (Farrell, 1972) as explained by Bos *et al.* (2015) over western Europe stations. Moreover, the effect of (sub-)daily signals on semi-annual and annual periodic signals from GPS observations (King *et al.*, 2008) can be reduced with combined GNSS solutions.

The unmodelled errors considered here are (very) large which arguably can be considered unrealistic. This was made in order to obtain measurable effects. Existing standard models will have smaller and more realistic errors than what we have assumed in this study. Nevertheless, the results demonstrate the sensitivity of GNSS constellation design and ground repeat periods on the propagation of unmodelled (sub-)daily tidal constituents into coordinates.

For this study, OTL is selected for simplicity and to see comparable effects with previous studies such as Penna *et al.* (2007). The unmodelled tidal constituent scenarios considered here can also be applied to the constituents of the same periods from solid Earth tides (e.g. Watson *et al.*, 2006) and/or atmospheric and other tidal effects in the geopotential and sub-daily EOPs and the propagation mechanisms investigated. A more detailed experiment such as Griffiths & Ray (2012) on how the (sub-)daily EOP tidal errors propagate into orbits for both GPS and GLONASS would help with understanding the effect.

ACKNOWLEDGEMENTS

KEA is funded by the Fonds National de la Recherche Luxembourg (contract number 6835562). We acknowledge the High Performance Computing (HPC) facility at the University of Luxembourg (https://hpc.uni.lu; Varrette *et al.*, 2014) for computational resources and the IGS, CODE and ESA for data and products. The suggestions for Fig. 1 and constructive comments from the editor, Duncan Agnew, are greatly appreciated. The very constructive reviews from Nigel Penna and an anonymous reviewer are also much appreciated.

REFERENCES

Abraha, K., Teferle, F., Hunegnaw, A. & Dach, R., 2017. GNSS related periodic signals in coordinate time-series from Precise Point Positioning, *Geophys. J. Int.,* **208**(3), 1449–1464.

Agnew, D.C. & Larson, K.M., 2007. Finding the repeat times of the GPS constellation, *GPS Solut.,* **11**(1), 71–76.

Amiri-Simkooei, A.R., Tiberius, C.C.J.M. & Teunissen, P.J.G., 2007. Assessment of noise in GPS coordinate time series: methodology and results, *J. geophys. Res.,* **112**(B7).

Arnold, D. *et al.*, 2015. CODE's new solar radiation pressure model for GNSS orbit determination, *J. Geod.,* **89**(8), 775–791.

Blewitt, G., Hammond, W.C., Kreemer, C., Plag, H.-P., Stein, S. & Okal, E., 2009. GPS for real-time earthquake source determination and tsunami warning systems, *J. Geod.,* **83**(3), 335–343.

Bos, M.S., Penna, N.T., Baker, T.F. & Clarke, P.J., 2015. Ocean tide loading displacements in western Europe: 2. GPS-observed anelastic dispersion in the asthenosphere, *J. geophys. Res.,* **120**(9), 6540–6557.

Bradley, S.L., Milne, G.A., Teferle, F.N., Bingley, R.M. & Orliac, E.J., 2009. Glacial isostatic adjustment of the British Isles: new constraints from GPS measurements of crustal motion, *Geophys. J. Int.,* **178**(1), 14–22.

Cartwright, D.E. & Tayler, R.J., 1971. New computations of the tide-generating potential, *Geophys. J. Int.,* **23**(1), 45–73.

Dach, R. *et al.*, 2009. GNSS processing at CODE: status report, *J. Geod.,* **83**(3-4), 353–365.

Dach, R., Lutz, S., Walser, P. & Fridez, P.E., 2015. *Bernese GNSS Software Version 5.2. User Nanual,* Astronomical Institute, University of Bern, Bern Open Publishing; ISBN: 978-3-906813-05-9.

Dong, D., Fang, P., Bock, Y., Cheng, M. & Miyazaki, S., 2002. Anatomy of apparent seasonal variations from GPS-derived site position time series, *J. geophys. Res.,* **107**(B4), ETG 9-1–ETG 9-16.

Dow, J.M., Neilan, R.E. & Rizos, C., 2009. The international GNSS service in a changing landscape of Global Navigation Satellite Systems, *J. Geod.,* **83**(3–4), 191–198.

Farrell, W.E., 1972. Deformation of the Earth by surface loads, *Rev. Geophys.,* **10**(3), 761–797.

Griffiths, J. & Ray, J., 2012. Sub-daily alias and draconitic errors in the IGS orbits, *GPS Solut.,* **17**(3), 413–422.

Kang, K., Wahr, J., Heflin, M. & Desai, S., 2015. Stacking global GPS verticals and horizontals to solve for the fortnightly and monthly body tides: implications for mantle anelasticity, *J. geophys. Res.,* **120**(3), 1787–1803.

King, M., 2006. Kinematic and static GPS techniques for estimating tidal displacements with application to Antarctica, *J. Geodyn.,* **41**(1), 77–86.

King, M.A., Watson, C.S., Penna, N.T. & Clarke, P.J., 2008. Subdaily signals in GPS observations and their effect at semiannual and annual periods, *Geophys. Res. Lett.,* **35**(3).

Martens, H.R., Simons, M., Owen, S. & Rivera, L., 2016. Observations of ocean tidal load response in South America from subdaily GPS positions, *Geophys. J. Int.,* **205**(3), 1637–1664.

Melgar, D. *et al.*, 2016. Local tsunami warnings: Perspectives from recent large events, *Geophys. Res. Lett.,* **43**(3), 1109–1117.

Penna, N.T. & Stewart, M.P., 2003. Aliased tidal signatures in continuous GPS height time series, *Geophys. Res. Lett.,* **30**(23), 2184 .

Penna, N.T., King, M.A. & Stewart, M.P., 2007. GPS height time series: Short-period origins of spurious long-period signals, *J. geophys. Res.,* **112**(B2).

Penna, N.T., Clarke, P.J., Bos, M.S. & Baker, T.F., 2015. Ocean tide loading displacements in western Europe: 1. Validation of kinematic GPS estimates, *J. geophys. Res.,* **120**(9), 6523–6539.

Petit, G. & Luzum, B., 2010. *IERS Conventions (2010), (IERS Technical Note 36) Frankfurt am Main: Verlag des Bundesamts für Kartographie und Geodäsie, 2010*. 179, ISBN 3-89888-989-6.

Ray, J., Altamimi, Z., Collilieux, X. & Dam, T., 2007. Anomalous harmonics in the spectra of GPS position estimates, *GPS Solut.,* **12**(1), 55–64.

Ray, J., Griffiths, J., Collilieux, X. & Rebischung, P., 2013. Subseasonal GNSS positioning errors, *Geophys. Res. Lett.,* **40**(22), 5854–5860.

Rebischung, P., Altamimi, Z., Ray, J. & Garayt, B., 2016. The IGS contribution to ITRF2014, *J. Geod.,* **90**(7), 611–630.

Rodriguez-Solano, C.J., Hugentobler, U., Steigenberger, P., Bloßfeld, M. & Fritsche, M., 2014. Reducing the draconitic errors in GNSS geodetic products, *J. Geod.,* **88**(6), 559–574.

Santamaría-Gómez, A., Gravelle, M., Collilieux, X., Guichard, M., Míguez, B.M., Tiphaneau, P. & W"oppelmann, G., 2012. Mitigating the effects of vertical land motion in tide gauge records using a state-of-the-art GPS velocity field, *Glob. Planet. Change,* **98–99,** 6–17.

Sella, G.F., Stein, S., Dixon, T.H., Craymer, M., James, T.S., Mazzotti, S. & Dokka, R.K., 2007. Observation of glacial isostatic adjustment in "stable" North America with GPS, *Geophys. Res. Lett.,* **34**(2), L02306 .

Stewart, M.P., Penna, N.T. & Lichti, D.D., 2005. Investigating the propagation mechanism of unmodelled systematic errors on coordinate time series estimated using least squares, *J. Geod.,* **79**(8), 479–489.

Susnik, A., Dach, R., Villiger, A., Maier, A., Arnold, D., Schaer, S. & Jäggi, A., 2016. *CODE Reprocessing Product Series,* Astronomical Institute, University of Bern .

Teferle, F.N., Bingley, R.M., Williams, S. & Dodson, A., 2006. Using continuous GPS and absolute gravity to separate vertical land movements and changes in sea-level at tide gauges in the UK, *Phil. Trans. R. Soc.,* **364,** 917–930.

Teferle, F.N. *et al.*, 2009. Crustal motions in Great Britain: evidence from continuous GPS, absolute gravity and Holocene sea level data, *Geophys. J. Int.,* **178**(1), 23–46.

Tregoning, P. & Watson, C., 2009. Atmospheric effects and spurious signals in GPS analyses, *J. geophys. Res.,* **114**(B9).

van Dam, T., Wahr, J., Milly, P.C.D., Shmakin, A.B., Blewitt, G., Lavallée, D. & Larson, K.M., 2001. Crustal displacements due to continental water loading, *Geophys. Res. Lett.,* **28**(4), 651–654.

Varrette, S., Bouvry, P., Cartiaux, H. & Georgatos, F., 2014. Management of an academic HPC cluster: the UL experience, in *Proceedings of the 2014 Intl. Conf. on High Performance Computing & Simulation (HPCS 2014),* Bologna, Italy, pp. 959–967.

Watson, C., Tregoning, P. & Coleman, R., 2006. Impact of solid Earth tide models on GPS coordinate and tropospheric time series, *Geophys. Res. Lett.,* **33**(8).

Yuan, L.G., Ding, X.L., Zhong, P., Chen, W. & Huang, D.F., 2009. Estimates of ocean tide loading displacements and its impact on position time series in Hong Kong using a dense continuous GPS network, *J. Geod.,* **83**(11), 999 .

Zumberge, J.F., Heflin, M.B., Jefferson, D.C., Watkins, M.M. & Webb, F.H., 1997. Precise point positioning for the efficient and robust analysis of GPS data from large networks, *J. geophys. Res.,* **102**(B3), 5005–5017.